Article

Photocatalytic Dehalogenation of Aromatic Halides on Ta2O5-Supported Pt-Pd Bimetallic Alloy Nanoparticles Activated by Visible Light

Hirokatsu Sakamoto, Jun Imai, Yasuhiro Shiraishi, Shunsuke Tanaka, Satoshi Ichikawa, and Takayuki Hirai

ACS Catal., **Just Accepted Manuscript** • DOI: 10.1021/acscatal.7b01735 • Publication Date (Web): 28 Jun 2017

Photocatalytic Dehalogenation of Aromatic Halides on Ta_2O_5-Supported Pt–Pd Bimetallic Alloy Nanoparticles Activated by Visible Light

Hirokatsu Sakamoto,[†] Jun Imai,[†] Yasuhiro Shiraishi,*[,†,‡] Shunsuke Tanaka,[‖] Satoshi Ichikawa,[§] and Takayuki Hirai[†]

[†] Research Center for Solar Energy Chemistry, and Division of Chemical Engineering, Graduate School of Engineering Science, Osaka University, Toyonaka 560-8531, Japan

[‡] Precursory Research for Embryonic Science and Technology (PRESTO), Japan Science and Technology Agency (JST), Saitama 332-0012, Japan

[‖] Department of Chemical, Energy and Environmental Engineering, Kansai University, Suita 564-8680, Japan

[§] Institute for NanoScience Design, Osaka University, Toyonaka 560-8531, Japan

ABSTRACT: Dehalogenation of aromatic halides is one important reaction for detoxification and organic synthesis. Photocatalytic dehalogenation with alcohol, a safe hydrogen source, is one promising method; however, early-reported systems need UV irradiation. We found that Pt–Pd bimetallic alloy nanoparticles (ca. 4 nm) supported on Ta_2O_5 (PtPd/Ta_2O_5), when absorbing visible light (λ >450 nm), efficiently promotes dehalogenation with 2-PrOH as a hydrogen source. Catalytic dehydrogenation of 2-PrOH on the alloy in the dark produces hydrogen atoms (H) on the particles. Photoexcitation of d electrons on the alloy particles by absorbing visible light produces hot electrons (e_{hot}^-). They efficiently reduce the adsorbed H atoms and produce hydride species (H^-) active for dehalogenation. The catalytic activity depends on the Pt/Pd mole ratio; alloy particles consisting of 70 mol % of Pt and 30 mol % Pd exhibit the highest activity for dehalogenation.

KEYWORDS: Photocatalysis· Visible light · Alloy nanoparticle · Hot electron · Dehalogenation

INTRODUCTION

Catalytic dehalogenation of aromatic halides is one of the very important reactions for detoxification and organic synthesis.[1,2] It is usually carried out on heterogeneous catalysts loaded with Pd or Rh nanoparticles with H_2 as a hydrogen source,[3–5] which holds potential explosion risks. Alternative method using a safe hydrogen source such as alcohols is desirable. Pd or Rh nanoparticles supported on carbon[6–8] or Fe_2O_3[9,10] promote the reaction with alcohol as a hydrogen source, but need relatively high temperature (>340 K). Design of catalytic system that efficiently promotes dehalogenation with alcohol at room temperature is desired.

Photocatalysis has also been studied extensively since it promotes dehalogenation with alcohols at room temperature under light irradiation.[11–14] Semiconductor TiO_2 loaded with Pd or Rh nanoparticles has been used as a catalyst with base such as NaOH.[15–20] Photoexcitation of the catalysts produces conduction band electrons (e_{CB}^-) and valence band holes (h_{VB}^+). The h_{VB}^+ oxidize alcohols and produce aldehydes (or ketones) and protons (H^+) (eq. 1). The H^+ are reduced by the e^- accumulated on the metal, producing hydrogen atoms (H–M) (eq. 2). They are further reduced with e^- (eq. 3), producing hydride species (H^-–M) active for dehalogenation (eq. 4). The removed Cl^- forms NaCl by the reaction with H^+ and NaOH (eq. 5). The overall reaction can be expressed as eq. 6.

$$RCH_2OH + 2h^+ \rightarrow RCHO + 2H^+ \quad (1)$$

$$H^+ + e^- + M \rightarrow H–M \quad (2)$$

$$H–M + e^- \rightarrow H^-–M \quad (3)$$

$$Ar–Cl + H^-–M \rightarrow Ar–H + Cl^- + M \quad (4)$$

$$Cl^- + H^+ + NaOH \rightarrow H_2O + NaCl\downarrow \quad (5)$$

$$Ar–Cl + RCH_2OH + NaOH \rightarrow Ar–H + RCHO + H_2O + NaCl\downarrow \quad (6)$$

These reactions proceed at room temperature with alcohol, and they enable safe, green, and sustainable dehalogenation. These early-reported systems, however, need UV light for catalyst photoexcitation. A new catalyst that promotes dehalogenation by visible light is therefore the most desired.

A metal nanoparticles/semiconductor system driven by light absorption of metal particles[21] is one promising system for

visible-light-driven photocatalysis, where Au[22–28] or Pt[29–32] particles supported on semiconductors such as TiO_2 have been used. In these systems, metal particles absorb light and produce *hot electrons* (e_{hot}^-) by the activation of their electrons.[33,34] The e_{hot}^- are injected into the semiconductor CB and the e_{CB}^- reduce substrates, while the positively-charged *hot holes* (δ^+) on the metal oxidize substrates, thus promoting photocatalytic reactions. Recently, we designed a new metal nanoparticles/semiconductor system; Pt particles supported on semiconductor Ta_2O_5 promote aerobic oxidation under visible light with significantly high quantum yield ~25 % (550 nm),[35] which is the highest yield among the systems reported earlier. As shown in Scheme 1, the Pt particles absorb visible light and produce e_{hot}^- via interband transition of d electrons (e_d^-). In this case, a high Schottky barrier (ϕ_B) is created at the Pt–Ta_2O_5 interface due to their large Fermi level difference.[36] The e_{hot}^- on Pt are therefore scarcely injected into the Ta_2O_5 CB. In contrast, strong Pt–Ta_2O_5 interaction leads to donation of Ta_2O_5 CB electrons to Pt particles and increases d electron density of the particles. This enhances interband transition and produces a large number of e_{hot}^-. Efficient e_{hot}^- donation to O_2 produces peroxide species active for oxidation, significantly enhancing aerobic oxidation.

Scheme 1. Aerobic oxidation on Pt/Ta_2O_5 under visible light.[a]

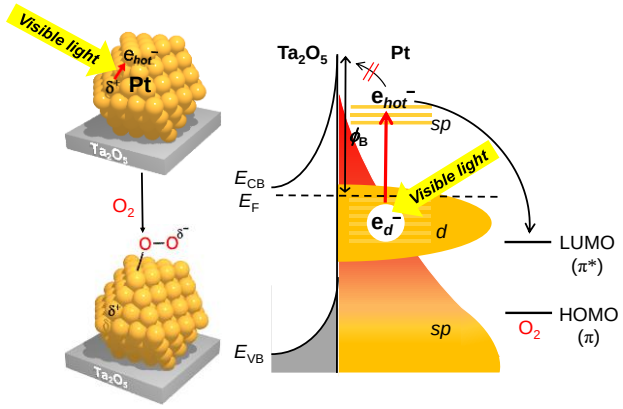

[a] E_F, Fermi level; ϕ_B [(eV) = $W - \chi$], height of Schottky barrier; W, work function of Pt (eV); χ, electron affinity of Ta_2O_5 (eV).

The present work aims at application of the Pt/Ta_2O_5 catalyst to photocatalytic dehalogenation with alcohol as a hydrogen source. We loaded Pt-Pd bimetallic alloy particles (ca. 4 nm) on Ta_2O_5. Visible light irradiation of the PtPd/Ta_2O_5 catalyst in 2-PrOH with NaOH efficiently promotes dehalogenation of aromatic halides. The photoreaction results and spectroscopic evidence revealed that catalytic dehydrogenation of 2-PrOH on the alloy particles in the dark produces H atoms. They are efficiently reduced by a large number of e_{hot}^- formed by interband transition of the alloy particles by absorbing visible light. This produces a large number of H^- species and enables highly efficient dehalogenation.

RESULTS AND DISCUSSION

Preparation and characterization of catalysts. The $Pt_{1-x}Pd_x/Ta_2O_5$ catalysts were prepared by two step procedures consisting of simultaneous impregnation of $H_2PtCl_6 \cdot 6H_2O$ and $Pd(NO_3)_2$ onto Ta_2O_5 [average diameter, 1.3 μm; surface area, 2.6 $m^2\ g^{-1}$] followed by H_2 reduction (see Experimental Section).[16,37] Total metal loadings on Ta_2O_5 were set at 8.8 mol % [= (Pt + Pd) / Ta_2O_5 × 100], and x denotes the mole fraction of Pd in the metal particles [x = Pd / (Pt + Pd)]. Transmission electron microscopy (TEM) observation of $Pt_{0.7}Pd_{0.3}/Ta_2O_5$ (Figure 1a and b) exhibits round and spherical metal particles with average diameter 3.8 nm. Figure 1c and d indicate that these particles can be indexed as face-centered cubic (*fcc*) structures. As shown in Figure S1 (Supporting Information), Pt_1/Ta_2O_5, $Pt_{0.5}Pd_{0.5}/Ta_2O_5$, and Pd_1/Ta_2O_5 contain metal particles with similar diameters (3.8, 3.5 and 4.0 nm, respectively), indicating that Pd alloying scarcely affects the particle diameter.

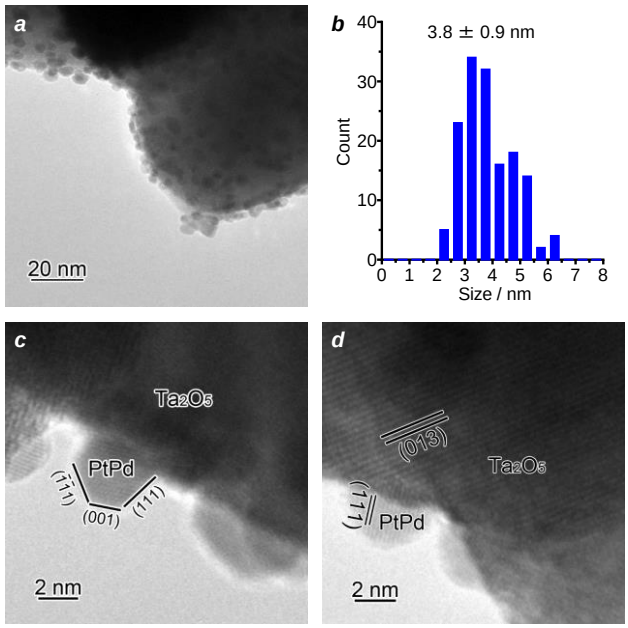

Figure 1. (a) TEM image of $Pt_{0.7}Pd_{0.3}/Ta_2O_5$ and (b) size distribution of alloy particles. (c, d) High-resolution images.

X-ray photoelectron spectroscopy (XPS) of the alloy catalysts (Figure S2, Supporting Information) reveals that Pt 4f, 4d, and Pd 3d peaks appear at the positions similar to those of Pt- or Pd-only catalysts because electronegativity of Pt (2.28) and Pd (2.22) are similar.[38,39] The Pt/Pd ratio of $Pt_{0.7}Pd_{0.3}/Ta_2O_5$ determined by XPS analysis is 2.38 mol/mol. This is similar to the mole ratio of total Pt and Pd amounts determined by the inductively coupled plasma (ICP) analysis (2.25 mol/mol) after dissolution of the catalyst with aqua regia. In addition, these ratios are close to the mole ratio of the Pt and Pd precursors (2.43 mol/mol). As shown in Figure 1c, d, the lattice spacing of the alloy particles (111) determined by TEM (0.226 nm) is in between that for standard Pt(111) (JCPDS 04-0802, 0.227 nm) and Pd(111) (JCPDS 05-0681, 0.225 nm), and is similar to the value calculated based on the Vegard's law (0.226 nm). These

findings clearly indicate that Pt and Pd components are mixed homogeneously. As shown in Figure 2a, diffuse-reflectance (DR) spectrum of Pt_1/Ta_2O_5 shows a broad absorption at λ >350 nm, assigned to interband transition of Pt.[40] Pd_1/Ta_2O_5 shows similar absorption assigned to light scattering by Pd particles.[16] The alloy catalysts therefore exhibit similar absorption regardless of their Pt/Pd ratios.

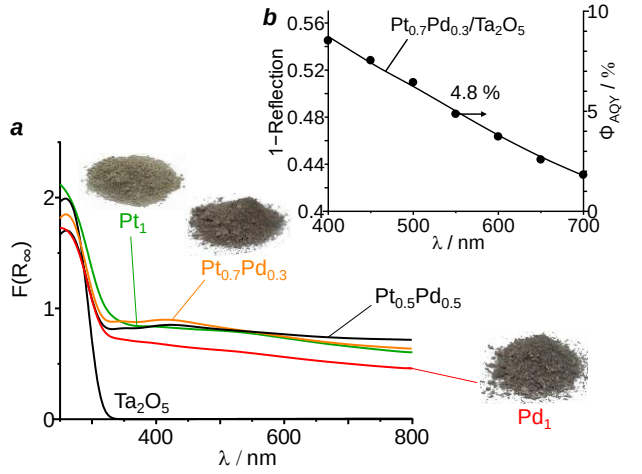

Figure 2. (a) DR UV-vis spectra of the catalysts and (b) action spectrum for photocatalytic dehalogenation of *p*-chlorotoluene on $Pt_{0.7}Pd_{0.3}/Ta_2O_5$. Apparent quantum yield for toluene formation (Φ_{AQY}) was determined with the equation: Φ_{AQY} (%) = [{(Y_{vis} – Y_{dark}) ×2} / (photon number entered into the reaction vessel)] × 100, where Y_{vis} and Y_{dark} are the toluene formed (μmol) under light irradiation and in the dark, respectively.

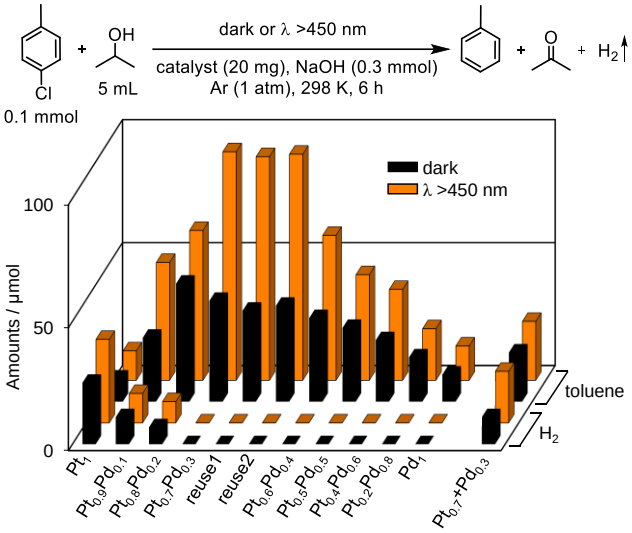

Figure 3. Amount of toluene and H_2 formed during the reaction of *p*-chlorotoluene on the respective catalysts for 6 h, (black) in the dark or (orange) under visible light irradiation (λ >450 nm; light intensity at 450–800 nm, 16.8 mW cm^{-2}). The reuse 1 and reuse 2 show the data obtained with $Pt_{0.7}Pd_{0.3}/Ta_2O_5$ catalyst when reused for further reactions. Catalysts were reused after simple washing with 2-PrOH followed by drying in vacuo.

Photocatalytic activity. Photocatalytic dehalogenation of *p*-chlorotoluene was performed. 2-PrOH (5 mL) containing *p*-chlorotoluene (0.1 mmol), catalyst (20 mg), and NaOH (0.3 mmol) was stirred under Ar atmosphere in the dark or under irradiation of visible light (λ >450 nm). The temperature of the solutions was maintained at 298 ± 0.5 K. Figure 3 summarizes the amount of toluene formed by 6 h reaction. In that, GC analysis of the solution for all systems detected only toluene and acetone as products. As shown by black bars, in the dark condition, Pt_1/Ta_2O_5 produces very small amount of toluene (9 μmol). Increasing Pd amount in the alloy increases the activity; $Pt_{0.8}Pd_{0.2}$ and $Pt_{0.7}Pd_{0.3}/Ta_2O_5$ catalysts produce relatively large amounts of toluene (ca. 40 μmol). Further Pd alloying, however, decreases the activity, where Pd_1/Ta_2O_5 produces very small amount of toluene (11 μmol).

As shown by orange bars (Figure 3), Pt_1/Ta_2O_5 shows almost no activity enhancement even under visible light irradiation. In contrast, the alloy catalysts enhance the activity, where $Pt_{0.7}Pd_{0.3}/Ta_2O_5$ produces the largest amount of toluene (93 μmol), which is twice that obtained in the dark. Further Pd alloying, however, decreases the activity. In addition, a physical mixture of $Pt_{0.7}/Ta_2O_5$ and $Pd_{0.3}/Ta_2O_5$ shows very low activity. These findings indicate that the Pt-Pd alloy containing small amount of Pd promotes dehalogenation efficiently under visible light. It must be noted that, as indicated by ″reuse 1 and 2″ in Figure 3, the $Pt_{0.7}Pd_{0.3}/Ta_2O_5$ catalyst recovered after the reaction, when reused for further reaction, produces 91 μmol and 92 μmol toluene, respectively, which are almost the same amounts obtained by the fresh catalyst (93 μmol). This indicates that the catalyst is reusable without loss of catalytic activity. It is also noted that ICP analysis of the solution recovered after the photoreaction does not detect Pt or Pd component. This indicates that leaching of these components from the alloy particles does not occur.

It is also noted that, as shown in Figure 3, Pt_1/Ta_2O_5 produces a large amount of H_2 during the reaction, although dehalogenation scarcely occurs. This is because, as shown in eq. 7, Pt has a low over potential for H_2 generation;[41] the H atoms produced on the particles are easily removed as H_2:

$$H–M + H–M \rightarrow H_2\uparrow + 2M \qquad (7)$$

In contrast, the alloy catalysts scarcely produce H_2 during the reaction. This indicates that they promote dehalogenation preferentially, while suppressing H_2 formation.

Figure 4 shows the time-dependent change in the amounts of substrate and products on $Pt_{0.7}Pd_{0.3}/Ta_2O_5$ during reaction of *p*-chlorotoluene under visible light. After 6 h photoreaction, *p*-chlorotoluene (100 μmol) is transformed to toluene (100 μmol) almost completely together with a formation of acetone (100 μmol). This indicates that, as shown by eq. 6, its –Cl group is removed stoichiometrically via the formation of toluene, acetone, and NaCl.[16] It is also noted that, after complete transformation of *p*-chlorotoluene to toluene (>6 h), H_2 starts to generate. This suggests that the alloy catalysts preferentially promote dehalogenation, while suppressing H_2 formation. As shown in Figure S3 (Supporting Information), similar tendency

is observed in the dark condition, although the dehalogenation rate is slower.

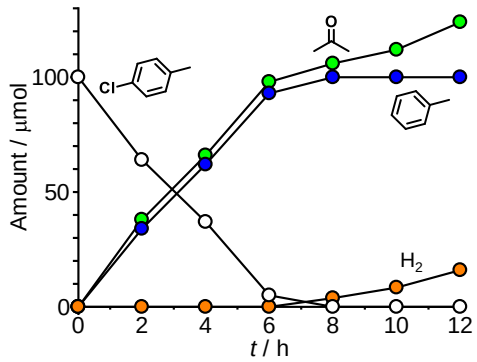

Figure 4. Time course for the amounts of substrates and products during reaction of *p*-chlorotoluene on $Pt_{0.7}Pd_{0.3}/Ta_2O_5$ under λ >450 nm irradiation.

Action spectrum for dehalogenation on $Pt_{0.7}Pd_{0.3}/Ta_2O_5$ obtained by monochromatic light irradiation is shown in Figure 2b. A good correlation is observed between the apparent quantum yields for toluene formation (Φ_{AQY}) and absorption spectrum of the catalyst. This clearly indicates that interband transition of d electrons on the alloy by absorbing visible light promotes dehalogenation. The $Pt_{0.7}Pd_{0.3}$ alloy particles loaded on TiO_2 ($Pt_{0.7}Pd_{0.3}/TiO_2$), when used for photocatalytic dehalogenation under visible light irradiation, produces only 8.1 μmol toluene, which is much lower than that of $Pt_{0.7}Pd_{0.3}/Ta_2O_5$ (93 μmol; Figure 3). This indicates that, as described in our Pt/Ta_2O_5 system,[35] d electron density of the alloy particles increased by strong interaction with Ta_2O_5 support enhances the interband transition of d electrons by visible light and produces a large number of e_{hot}^-, leading to efficient dehalogenation.

Dehalogenation mechanism. The dehalogenation proceeds via the three steps consisting of (i) formation of H atoms on the metal surface by dehydrogenation of 2-PrOH, (ii) formation of H^- species by the reduction of H atoms, and (iii) dehalogenation by the H^- species. The mechanism on the $PtPd/Ta_2O_5$ catalyst can be explained by Scheme 2. In the first step (a), 2-PrOH is adsorbed on the metal and undergoes dehydrogenation in the dark condition, producing acetone and H atoms. In the dark, the adsorbed H atoms are reduced by the d electrons (e_d^-) of metal and produce H^- species (b):

$$H–PtPd + e_d^- \rightarrow H^–PtPd \quad (8)$$

Upon visible light irradiation, interband transition of e_d^- on the metal produces a large number of e_{hot}^- and δ^+ pairs (c).

$$H–PtPd + h\nu \rightarrow H–PtPd\ (e_{hot}^- + \delta^+) \quad (9)$$

The e_{hot}^- reduce the adsorbed H atoms and create a large number of H^- (d), where the δ^+ on the metal are consumed by oxidation of 2-PrOH.

$$H–PtPd + e_{hot}^- \rightarrow H^–PtPd \quad (10)$$

$$1/2RCH_2OH + \delta^+ \rightarrow 1/2RCHO + H^+ \quad (11)$$

Nucleophilic addition of H^- to aromatic halide (e) promotes dehalogenation (eq. 4). The removed Cl^- are solidified by the reaction with H^+ and NaOH (eq. 5).

Scheme 2. Possible mechanism for dehalogenation on $PtPd/Ta_2O_5$.

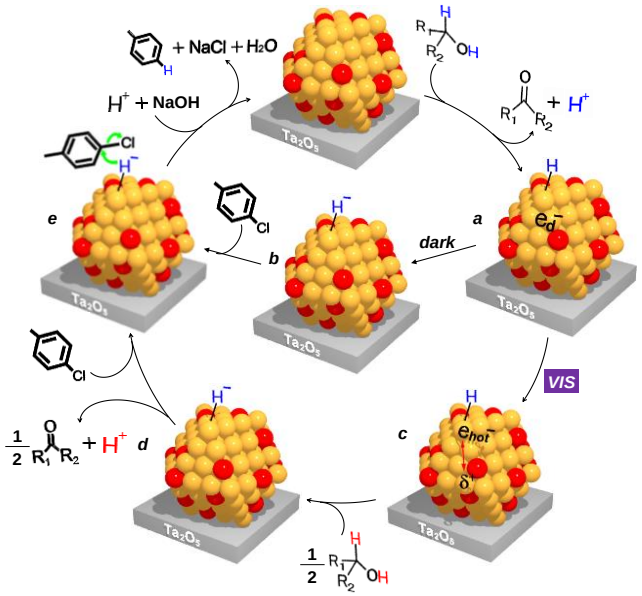

Dehydrogenation of 2-PrOH. As shown in Scheme 2a, the first step of dehalogenation is the dehydrogenation of 2-PrOH, producing H atoms on the metal surface. The reaction occurs ″in the dark″. This is confirmed by the reaction of 2-PrOH without *p*-chlorotoluene. Figure 5 shows the amount of acetone formed in the dark or under visible light. In both cases, Pt_1/TiO_2 shows the highest activity, and the activity decreases by the Pd alloying. The rate-determining step for this reaction is the H abstraction of alcohol on the metal,[42,43] and its activity depends on the position of metal d-band center relative to their Fermi levels.[44] As shown in Scheme 3a, adsorption of alcohol onto the metal creates bonding (σ) and antibonding (σ*) states between the d-band center and HOMO and LUMO of alcohol, respectively.[45,46] The HOMO electrons of alcohol are donated to the bonding state and undergoes dehydrogenation.[47] The d-band center of Pt and Pd lies at –2.2 and –1.8 eV, respectively,[48] indicating that Pd creates upper-shifted bonding state. This suppresses electron donation from HOMO of 2-PrOH to the bonding state and shows lower dehydrogenation activity than Pt (Figure 5). Increasing amount of Pd alloying leads to upper-shift of the d-band center[48] and decreases the dehydrogenation activity. It is note that, as shown in Figure 5, the amount of acetone formed under visible light (orange) is similar to that formed in the dark (black). This means that e_{hot}^- formed on the metal by light absorption scarcely enhances dehydrogenation of 2-PrOH. These results clearly suggest that, during

dehalogenation, the H atoms are mainly produced by the dark reaction. It is also noted that Pd_1/Ta_2O_5 produces very small amount of acetone (Figure 5). This suggests that very low dehalogenation activity of Pd_1/Ta_2O_5 (Figure 3) is due to the low activity of dehydrogenation of 2-PrOH, producing very small amount of H atoms on the surface.

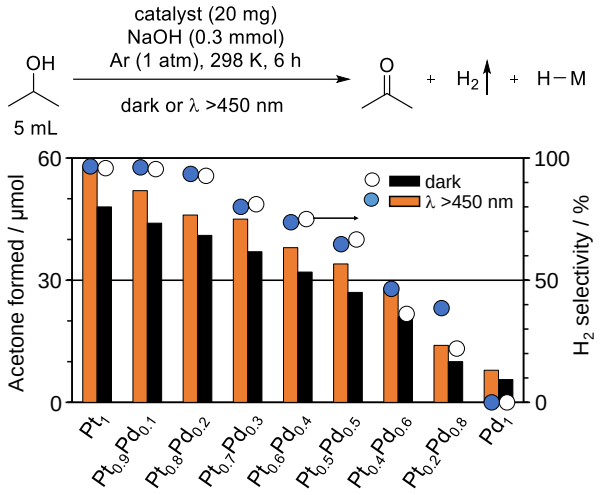

Figure 5. Formation of acetone by dehydrogenation of 2-PrOH on $Pt_{0.7}Pd_{0.3}/Ta_2O_5$ at 298 K. The selectivity for H_2 formation defined by eq. 12 was also shown in the figure.

Formation of H^- in the dark. The second step for dehalogenation is the reduction of H atoms on the metal, producing H^- species active for dehalogenation. In the dark, as shown in Figure 3, Pt_1/Ta_2O_5 shows very low dehalogenation activity, although H atoms are produced efficiently by the enhanced dehydrogenation of 2-PrOH (Figure 5). This is because the formed H atoms are readily removed as H_2 gas due to the weak H–M interaction. Figure 5 (right) shows the H_2 selectivity defined as the ratio of the amount of formed H_2 to that of formed acetone, as follows:

$$H_2 \text{ selectivity } (\%) = [H_2] / [\text{acetone}] \times 100 \qquad (12)$$

The H_2 selectivity on Pt_1/Ta_2O_5 is almost 100%, indicating that the formed H atoms are readily removed as H_2. This can be explained by the lower d-band center of Pt. As shown in Scheme 3b, the H atoms adsorbed on the Pt surface creates antibonding state at a level relatively lower than the Fermi level; therefore, this state is occupied by the electrons. This weakens H–Pt interaction and allows H_2 generation (eq. 7), which is related to the lower over potential for H_2 generation on Pt.[49] In contrast, as shown in Figure 5, the H_2 selectivity decreases with an increase in the Pd amount within the alloy. This means that the H atoms formed on the metal surface remain without H_2 formation. This is because, as shown in Scheme 3b, the Pd d-band center lies at upper level. This strengthens H–M interaction and suppresses H_2 generation.[50,51] This therefore promotes efficient donation of d electrons to the bonding state and produces H^- species. However, as shown in Figure 3, Pd_1/Ta_2O_5 shows very low dehalogenation activity in the dark. This is because it is less active for dehydrogenation of 2-PrOH and scarcely produces H atoms on the surface. The $PtPd/Ta_2O_5$ alloy catalysts promote dehydrogenation of 2-PrOH (formation of H atoms) relatively efficiently and stabilizes the H atoms by relatively strong H–M binding. This reduces the H atoms efficiently (formation of H^-) and promotes efficient dehalogenation in the dark.

Scheme 3. Energy diagram for the electronic states of (a) metal–alcohol and (b) metal–H bonding.

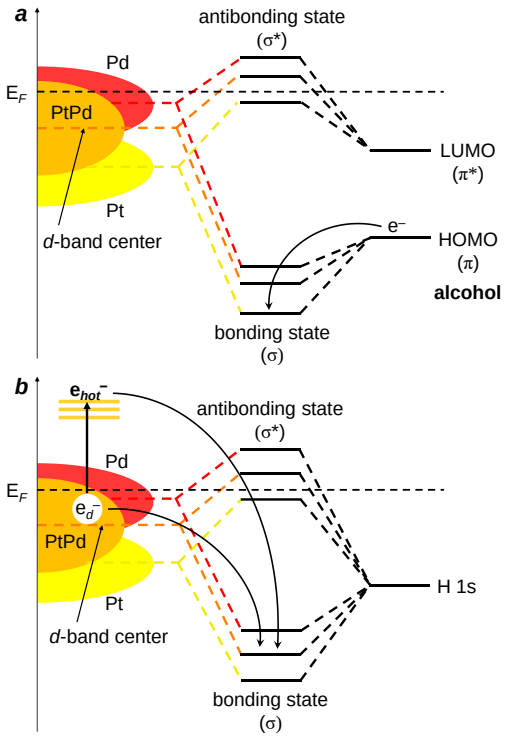

Formation of H^- under visible light. Upon visible light irradiation, $PtPd/Ta_2O_5$ shows much enhanced dehalogenation activity than that in the dark (Figure 3). This is because the H atoms on the metal particles are efficiently reduced by the photogenerated e_{hot}^-, producing a large number of H^- that promotes efficient dehalogenation.[15–20] As shown in Figure 6, diffuse-reflectance infrared Fourier transform (DRIFT) analysis of H_2-adsorbed $Pt_{0.7}Pd_{0.3}/Ta_2O_5$ confirms this. H_2 adsorbed in the dark (black) shows a band at 1963 cm^{-1} for the H–M species.[52] Visible light irradiation of the sample (blue), however, shows a red-shifted band at 1948 cm^{-1}. This suggests that negatively-charged H^- species, which are adsorbed on the metal surface more strongly than H atoms,[53] are indeed generated by visible light irradiation. This indicates that, as shown in Scheme 3b, the donation of e_{hot}^- on the alloy to the bonding state of the adsorbed H atoms indeed produces H^- efficiently. As a result of this, a large number of H^- formed by visible light irradiation enhances dehalogenation of aromatic halides (Figure 3).

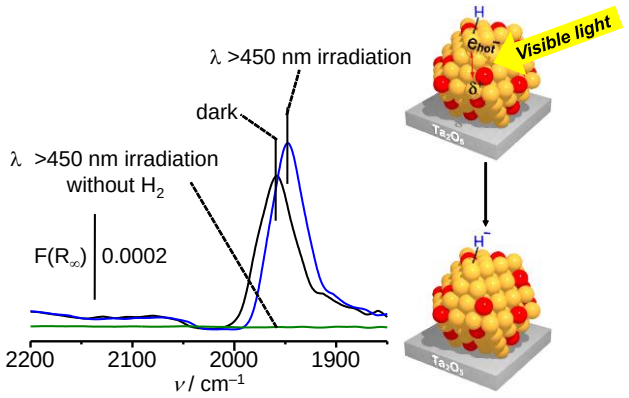

Figure 6. DRIFT spectra of H_2-adsorbed $Pt_{0.7}Pd_{0.3}/Ta_2O_5$ measured at 303 K (black) in the dark and (blue) after 450 nm light irradiation. Catalyst (20 mg) was evacuated (6.8×10^{-3} Torr) at 423 K for 3 h. H_2 (15 Torr) was added and left for 1 h in the dark or under photoirradiation. Green line shows the spectrum obtained at 303 K after photoirradiation without H_2.

Dehalogenation of aromatic halides. The $Pt_{0.7}Pd_{0.3}/Ta_2O_5$ catalyst was used for dehalogenation of substituted aromatic halides. As listed in Table 1, several aryl chlorides and bromides are transformed to the dehalogenated products with more than 89 % yields, while maintaining the substituents. As shown in Scheme 4, the dehalogenation step involves two consecutive reactions consisting of (i) nucleophilic addition of H^- to aromatic halide, and (ii) abstraction of Cl^- from the intermediate. To clarify its kinetics, Hammett plot analysis[54] was carried out. Dehalogenation of chlorobenzene (**1**) and some *p*-substituted ones (**2**, **6**, and **7**) was performed on $Pt_{0.7}Pd_{0.3}/Ta_2O_5$ for 1 h in the dark or light irradiation condition. The obtained first-order rate constants, k (mM h^{-1}), are shown in Table S1 (Supporting Information). Figure 7 plots the log$k$ versus the substituent constant, σ.[55] Almost identical relationship is observed in both conditions with the slope (Hammett constant, ρ) –0.96. The results clearly indicate that dehalogenation in the both conditions proceeds via the same mechanism consisting of (i) nucleophilic H^- addition and (ii) abstraction of Cl^-, as summarized in Scheme 4.

The negative ρ indicates that electron-donating substituents accelerate dehalogenation, although nucleophilic H^- addition (step i) is accelerated by electron-withdrawing substituents.[56] This is because the abstraction of Cl^- (step ii) is the rate-determining step; this occurs slowly in the present system operated at room temperature. The Cl^- abstraction is accelerated by the electron-donating substituents because they stabilize the negative charge of intermediate.[57] This therefore results in negative ρ for the present systems (Figure 7). Visible light irradiation enhances the H^- formation by photogenerated e_{hot}^- and efficiently promotes the first step (nucleophilic addition of H^- to aromatic halides). This produces a large number of the H-adduct intermediates and accelerates the second step (Cl^- abstraction) accordingly.

Table 1. Dehalogenation results on $Pt_{0.7}Pd_{0.3}/Ta_2O_5$.[a]

No.	substrate	light	time / h	product	Yield / %[b]
1		+	12		>99
		–			66
2	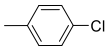	+	6		95
		–			43
3	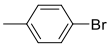	+	6		>99
		–			55
4		+	6		>99
		–			43
5	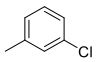	+	8		98
		–			63
6	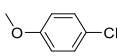	+	5		98
		–			66
7	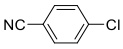	+	96		>99
		–			74
8		+	12		89
		–			59
9	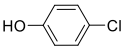	+	24		91
		–			55
10		+	24		89
		–			63
11		+	12		91
		–			68
12		+	24		89
		–			62

[a] Reaction conditions: 2-PrOH (5 mL), substrate (0.1 mmol), NaOH (0.3 mmol), catalyst (20 mg), Ar (1 atm), in the dark or under visible light irradiation, temperature (298 K). [b] = (product formed) / (initial amount of substrate) × 100.

Scheme 4. Mechanism for dehalogenation by H^- species.

Effect of the alloy amount. The activity of $Pt_{0.7}Pd_{0.3}/Ta_2O_5$ catalyst depends on the loaded amount of alloy particles. This is confirmed by the dehalogenation reactions on the $Pt_{0.7}Pd_{0.3}/Ta_2O_5$ catalysts with different loadings of $Pt_{0.7}Pd_{0.3}$ alloy [(Pt + Pd) / Ta_2O_5 × 100 = 2.2, 4.4, 8.8, and 13 mol %].

As shown in Figure 8 (blue), the sizes of alloy particles on the respective catalysts are similar (3.7–4.0 nm). The black and orange bars show the amounts of toluene formed in the dark and under photoirradiation, respectively. The dark activity increases with the alloy loadings because the increased surface area of alloy produces larger number of H^-. Photoirradiation further enhances the reaction, but the enhancement depends on the alloy amount; low-alloy-loading catalysts show small enhancement, but high-alloy-loading catalysts shows large enhancement. As shown in Figure S4 (Supporting Information), absorbance of alloy particles in the visible region decreases with a decrease in the alloy loadings. This indicates that efficient light absorption by the alloy particles is the important factor for photocatalytic dehalogenation.

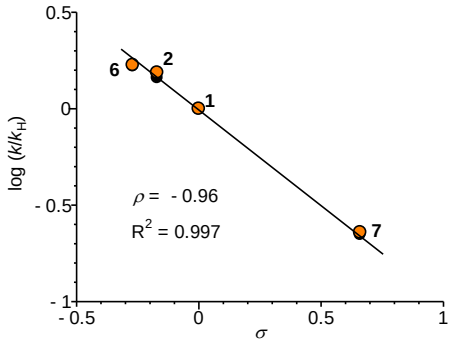

Figure 7. Hammett plot for dehalogenation of some *p*-substituted chlorobenzenes on $Pt_{0.7}Pd_{0.3}/Ta_2O_5$ (black) in the dark or (orange) under photoirradiation. The *k* denotes the first-order rate constant for dehalogenation (mM h^{-1}) determined by 1 h reaction. The reaction conditions are identical to those in Figure 3.

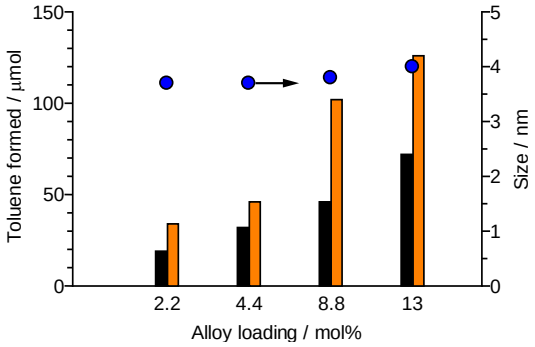

Figure 8. Effect of the loaded amount of $Pt_{0.7}Pd_{0.3}$ alloy on the toluene formation by dehalogenation of *p*-chlorotoluene (6 h reaction). Circles show average sizes of $Pt_{0.7}Pd_{0.3}$ alloy on the catalysts determined by TEM (Figure S1, Supporting Information). Reaction conditions: 2-PrOH (5 mL), substrate (0.2 mmol), NaOH (0.5 mmol), catalyst (20 mg), Ar (1 atm), in the dark or under visible light, temperature (298 K). In all runs, H_2 was scarcely detected, indicating that H atoms of 2-PrOH are selectively used for dehalogenation.

CONCLUSION

We found that Pt-Pd bimetallic alloy particles supported on Ta_2O_5 efficiently promote photocatalytic dehalogenation under visible light at room temperature with 2-PrOH as a hydrogen source. The alloy particles absorbing visible light promote interband transition of d electrons and produces large number of e_{hot}^-. The e_{hot}^- efficiently reduce the H atoms produced by dehydrogenation of 2-PrOH and produce H^- species active for dehalogenation. The activity depends on the Pt/Pd ratio; the alloy particles consisting of 70 mol % Pt and 30 mol % Pd exhibit the highest activity. The basic concept presented here based on efficient formation of H^- by the photogenerated e_{hot}^- on the metal under visible light may contribute to the creation of more efficient photocatalytic system for dehalogenation and to the design of new system for sunlight-driven selective organic transformations.

EXPERIMENTAL SECTION

Catalyst preparation. Ta_2O_5 particles were supplied from Wako. $Pt_{1-x}Pd_x/Ta_2O_5$ catalysts with metal loadings 8.8 mol % [x = Pd/(Pt + Pd); x = 0, 0.1, 0.2, 0.3, 0.4, 0.5, 0.6, 0.8, and 1] were prepared as follows: Ta_2O_5 (1 g) was added to water (40 mL) containing $H_2PtCl_6 \cdot 6H_2O$ and $Pd(NO_3)_2$ [57/0, 50/2, 44/5, 39/7, 33/10, 11/20, and 0/25 mg/mg, respectively]. Water was removed by evaporation at 353 K with vigorous stirring for 12 h. The obtained powders were reduced under H_2 flow at 673 K (heating rate, 2 K min^{-1}; holding time at 673 K, 2 h). $Pt_{0.7}Pd_{0.3}/TiO_2$ catalyst was prepared using P25 TiO_2 (JRC-TIO-4), kindly supplied from the Catalyst Society of Japan, in a manner similar to that of $Pt_{0.7}Pd_{0.3}/Ta_2O_5$.

Photoreaction. 2-PrOH (5 mL) containing catalyst (20 mg), *p*-chlorotoluene (0.1 mmol), and NaOH (0.3 mmol) were added to a Pyrex glass tube (φ 12 mm; capacity, 20 mL). The tube was sealed with a rubber cap and purged with Ar gas (5 min). The tube was set in a water bath, whose temperature was kept digitally at 298 ± 0.5 K.[22] The tube was irradiated at λ >450 nm under magnetic stirring by a 2 kW Xe lamp (USHIO Inc.) in a manner similar to that of our Pt/Ta_2O_5 system.[35] After the reaction, the gas phase was analyzed by GC-BID (Shimadzu, GC-2010 plus). The catalyst was recovered by centrifugation, and the resulting solution was analyzed by GC-FID (Shimadzu, GC-2010). The substrate and product amounts were calibrated with authentic samples. All reactions and analysis were performed twice, where the errors were less than 1%. Action spectrum was obtained by the reaction in 2-PrOH (2 mL) containing catalyst (8 mg), *p*-chlorotoluene (0.2 mmol), and NaOH (0.5 mmol) with monochromated light.[58]

Analysis. DRIFT spectra were measured on a FT/IR-610 system (JASCP Corp.),[59] where 450 nm light was irradiated by a Xe lamp (300 W; Asahi Spectra Co. Ltd.; Max-302; light intensity, 68 μW cm^{-2}). Spectral irradiance of the light sources are shown in Figure S5 (Supporting Information). TEM observations,[60] XRD, XPS, and DR UV-vis measurements were performed according to the procedure described previously.[61]

ASSOCIATED CONTENT

Parameter for Hammett analysis (Table S1), TEM images and size distribution of alloy particles (Figure S1), XPS charts (Figure S2), Time profiles for the dehalogenation reaction in the dark (Figure S3), DR UV-vis spectra (Figure S4), Spectral irradiance of light sources (Figure S5). This material is available free of charge via the Internet at http://pubs.acs.org.

AUTHOR INFORMATION

Corresponding Author

shiraish@cheng.es.osaka-u.ac.jp

Notes

The authors declare no competing financial interest.

ACKNOWLEDGMENT

This work was supported by the Grant-in-Aid for Scientific Research (No. 26289296) from the Ministry of Education, Culture, Sports, Science and Technology, Japan (MEXT).

REFERENCES

(1) Alonso, F.; Beletskaya, I. P.; Yus, M. *Chem. Rev.* **2002**, *102*, 4009–4092.
(2) Grushin, V. V.; Alper, H. *Chem. Rev.* **1994**, *94*, 1047–1062.
(3) Lapierre, R. B.; Guczi, L.; Kranich, W. L.; Weiss, A. H. *J. Catal.* **1978**, *52*, 230–238.
(4) Hara, T.; Kaneta, T.; Mori, K.; Mitsudome, T.; Mizugaki, T.; Ebitani, T.; Kaneda, K. *Green Chem.* **2007**, *9*, 1246–1251.
(5) Yuan, G.; Keane, M. A. *Ind. Eng. Chem. Res.* **2007**, *46*, 705–715.
(6) Ukisu, Y.; Iimura, S.; Uchida, R. *Chemosphere* **1996**, *33*, 1523–1530.
(7) Miyadera, T.; Ukisu, Y. *J. Mol. Catal. A* **1997**, *125*, 135–142.
(8) Ukisu, Y. *React. Kinet., Mech. Catal.* **2015**, *114*, 385–394.
(9) Patra, A. K.; Dutta, A.; Bhaumik, A. *Appl. Mater. Interfaces* **2012**, *4*, 5022–5028.
(10) Peĺisson, C.-H.; Nowicki, A. D.; Roucoux, A. *ACS Sus. Chem. Eng.* **2016**, *4*, 1834–1839.
(11) Choi, W.; Hoffmann, M. R. *Environ. Sci. Technol.* **1995**, *29*, 1646–1654.
(12) Sun, C.; Zhao, J.; Ji, H.; Ma, W.; Chen, C. *Chemoshere* **2012**, *89*, 420–425.
(13) Chang, W.; Cun, S.; Pang, X.; Sheng, H.; Li, Y.; Ji, H.; Song, W.; Chen, C.; Ma, W.; Zhao, J. *Angew. Chem., Int. Ed.* **2015**, *54*, 2052–2056.
(14) Sun, C.; Zhao, D.; Chen, C.; Ma, W.; Zhao, J. *Environ. Sci. Technol.* **2009**, *43*, 157–162.
(15) Fuku, K.; Hashimoto, K.; Kominami, H. *Chem. Commun.* **2010**, *46*, 5118–5120.
(16) Shiraishi, Y.; Takeda, Y.; Sugano, Y.; Ichikawa, S.; Tanaka, S.; Hirai, T. *Chem. Commun.* **2011**, *47*, 7863–7865.
(17) Yin, H.; Wada, Y.; Kitamura, T.; Yanagida, S. *Environ. Sci. Technol.* **2001**, *35*, 227–231.
(18) Kuchmii, S. Y.; Korzhak, A. V.; Kryukov. A. I. *Theor. Exp. Chem.* **1999**, *35*, 153–157.
(19) Zahran, E. M.; Bedford, N. M.; Nguyen, M. A.; Chang, Y. J.; Guiton, B. S.; Naik, R. R.; Bachas, L. G.; Knecht, M. R. *J. Am. Chem. Soc.* **2014**, *136*, 32–35.
(20) Nguyen, M. A.; Zahran, E. M.; Wilbon, A. S.; Besmer, A. V.; Cendan, V. J.; Ranson, W. A.; Lawrence, R. L.; Cohn, J. L.; Bachas, L. G.; Knecht, M. R. *ACS Omega* **2016**, *1*, 41–51.
(21) Tian, Y.; Tatsuma, T. *J. Am. Chem. Soc.* **2005**, *127*, 7632–7637.
(22) Tsukamoto, D.; Shiraishi, Y.; Sugano, Y.; Ichikawa, S.; Tanaka, S.; Hirai, T. *J. Am. Chem. Soc.* **2012**, *134*, 6309–6315.
(23) Sugano, Y.; Shiraishi, Y.; Tsukamoto, D.; Ichikawa, S.; Tanaka, S.; Hirai, T. *Angew. Chem., Int. Ed.* **2013**, *52*, 5295–5299.
(24) Primo, A.; Corma, A.; García, H. *Phys. Chem. Chem. Phys.* **2011**, *13*, 886–910
(25) Jia, H.; Zhu, X.-M.; Jiang, R.; Wang, J. *ACS Appl. Mater. Interfaces* **2017**, *9*, 2560–2571.
(26) Tanaka, A.; Hashimoto, K.; Kominami, H. *J. Am. Chem. Soc.* **2012**, *134*, 14526–14533.
(27) Kumar, D.; Lee, A.; Lee, T.; Lim, M.; Lim, D.-K. *Nano Lett.* **2016**, *16*, 1760–1767.
(28) Zhang, Z.; Li, A.; Cao, S.-W.; Bosman, M.; Li, S. *Nanoscale* **2014**, *6*, 5217–5222.
(29) Shiraishi, Y.; Tsukamoto, D.; Sugano, Y.; Shiro, A.; Ichikawa, S.; Tanaka, S.; Hirai, T. *ACS Catal.* **2012**, *2*, 1984–1992.
(30) Zai, W.; Xue, S.; Zhu, A.; Luo, Y.; Tian, Y. *ChemCatChem* **2011**, *3*, 127–130.
(31) Shiraishi, Y.; Sakamoto, H.; Fujiwara, K.; Ichikawa, S.; Hirai, T. *ACS Catal.* **2014**, *4*, 2418–2425.
(32) Shiraishi, Y.; Sakamoto, H.; Sugano, Y.; Ichikawa, S.; Hirai, T. *ACS Nano* **2013**, *7*, 9287–9297.
(33) Singh, J.; Singh, N. *Phys. Rev. B* **1978**, *18*, 2954–2960.
(34) Bobyrev, Y. V.; Petnikova, V. M.; Rudenko, K. V.; Shuvalov, V. V. *Quantum Electron.* **2002**, *32*, 789–792.
(35) Sakamoto, H.; Ohara, T.; Yasumoto, N.; Shiraishi, Y.; Ichikawa, S.; Tanaka, S.; Hirai, T. *J. Am. Chem. Soc.* **2015**, *137*, 9324–9332.
(36) Chun, W.-J.; Ishikawa, A.; Fujisawa, H.; Takata, T.; Kondo, J.; Hara, M.; Kawai, M.; Matsumoto, Y.; Domen, K. *J. Phys. Chem. B* **2003**, *107*, 1798–1803.
(37) Shiraishi, Y.; Ikeda, M.; Tsukamoto, D.; Tanaka, S.; Hirai, T. *Chem. Commun.* **2011**, *47*, 4811–4813.
(38) Trasatti, S. *J. Electroanal. Chem.* **1971**, *33*, 351–378.
(39) Watson, R. E.; Bennett, L. H. *Phys. Rev. B* **1978**, *18*, 6439–6448.
(40) Bigall, N. C.; Härtling, T.; Klose, M.; Simon, P.; Eng, L. M.; Eychmüller, A. *Nano Lett.* **2008**, *8*, 4588–4592.
(41) Guo, X.-C.; Madix, R. J. *J. Catal.* **1995**, *155*, 336–344.
(42) Meng, N.; Ando, Y.; Shinoda, S.; Saito, Y. *Bull. Chem. Soc. Jpn.* **1999**, *72*, 669–672.
(43) Ukisu, Y.; Miyadera, T. *React. Kinet. Catal. Lett.* **2004**, *81*, 305–311.
(44) Delbecq, F.; Sautet, P. *J. Catal.* **2003**, *220*, 115–126.
(45) Hammer, B.; Norckov, J. K. *Nature* **1995**, *376*, 238–240.
(46) Ghosh, D. C.; Jana, J. *Int. J. Quantum Chem.* 2003, 92, 484–505.
(47) Cheng, Z.; Wang, J.-H.; Choi, Y. M.; Yang, L.; Lin, M. C.; Liu, M. *Energy Environ. Sci.* **2011**, *4*, 4380–4409.
(48) Shao, M.; Liu, P.; Zhang, J.; Adzic, R. *J. Phys. Chem. B* **2007**, *111*, 6772–6775.
(49) Wilde, M.; Fukutani, K.; Ludwig, W.; Brandt, B.; Fischer, J.–H.; Schauermann, S.; Freund, H.–J. *Angew. Chem., Int. Ed.* **2008**, *47*, 9289–9283.
(50) Murillo, L. E.; Goda, A. M.; Chen, J. G. *J. Am. Chem. Soc.* **2007**, *129*, 7101–7105.
(51) Nørskov, J. K.; Bligaard, T.; Rossmeisl, J.; Christensen, C. H. *Nat. Chem.* **2009**, *1*, 37–46.
(52) Jayasooriya, U. A.; Chesters, M. A.; Howard, M. W.; Kettle, S. F. A.; Powell D. B.; Sheppard, N. *Surf. Sci.* **1980**, *93*, 526–534.
(53) Kaesz, H. D.; Saillant, R. B. *Chem. Rev.* **1972**, *72*, 231–281.
(54) Hartley, J. H.; Phillips, M. D.; James, T. D. *New J. Chem.* **2002**, *26*, 1228–1237.
(55) Hansch, C.; Leo, A.; Taft, R. W. *Chem. Rev.* **1991**, *91*, 165–195.
(56) Larsen, J.; Jørgensen, K. A. *J. Chem. Soc., Perkin Trans. 2* **1992**, *8*, 1213–1215.
(57) Cho, B. R.; Pyun, S. Y. *J. Am. Chem. Soc.* **1991**, *113*, 3920–3924.

(58) Shiraishi, Y.; Tanaka, K.; Shirakawa, E.; Sugano, Y.; Ichikawa, S.; Tanaka, S.; Hirai, T. *Angew. Chem., Int. Ed.* **2013**, *52*, 8304–8308.
(59) Hirakawa, H.; Katayama, M.; Shiraishi, Y.; Sakamoto, H.; Wang, K.; Ohtani, B.; Ichikawa, S.; Hirai, T. *ACS Appl. Mater. Interfaces* **2015**, *7*, 3797–3806.
(60) Kofuji, Y.; Isobe, Y.; Shiraishi, Y.; Sakamoto, H.; Tanaka, S.; Ichikawa, S.; Hirai, T. *J. Am. Chem. Soc.* **2016**, *138*, 10119–10025.
(61) Kofuji, Y.; Ohkita, S.; Shiraishi, Y.; Sakamoto, H.; Tanaka, S.; Ichikawa, S.; Hirai, T. *ACS Catal.* **2016**, *6*, 7021–7029.